AIAA JOURNAL
Vol. 34, No. 6, June 1996

Particle Size Distribution Technique Using Conventional Laser Doppler Velocimetry Measurements

Mark S. Maurice*
U.S. Air Force Wright Laboratory, Wright–Patterson Air Force Base, Ohio 45433-7005

The difference between the particle velocity and the fluid velocity within a flowfield is a direct function of the particle size distribution. Utilizing classical particle behavior through an oblique shock, a numerical algorithm has been developed to extract a size distribution estimate from conventional laser Doppler velocimetry (LDV) measurements. As a specific application, the method is used to determine the size distribution of atomized silicon oil seed from LDV measurements through the leading-edge shock of a hypersonic forebody inlet at Mach 5.76. Knowledge of the particle sizes allows the measurement bias to be quantified and removed, thereby greatly enhancing the value of LDV as a nonintrusive flowfield measurement technique.

Nomenclature

A, B	= coefficient matrices
a, b	= matrix coefficients
BW	= velocity histogram bin width
C	= particle size concentration matrix
C_d	= drag coefficient, Eq. (2)
C_{d1}	= function defined by Eq. (3)
c	= concentration of particle size
d	= particle diameter
d/s	= fluid velocity downstream of shock wave
G	= Gaussian function defined by Eq. (7)
g	= function defined by Eq. (4)
h	= function defined by Eq. (5)
M	= Mach number
M	= number of measurements in a histogram bin
m	= normalized histogram bin height
n	= upper limit number
R	= residual between measured and computational velocities
Re	= Reynolds number
T	= temperature
t	= time
u/s	= fluid velocity upstream of shock wave
V	= velocity component
$\bar{V}$	= mean velocity
X	= spatial coordinate (in direction of subscript)
γ	= ratio of specific heats
ρ	= density
σ	= standard deviation

Subscripts

BIN	= velocity histogram bin
f	= fluid velocity
i	= histogram bin index
j	= measurement station index
k, l	= seed diameter index
N	= normal component
p	= particle property
POINTS	= measurement stations
R	= the relative difference between the particle and the fluid
SEED	= seed size
SETS	= possible equation sets
SHOCK	= relative to the shock orientation
T	= tangential component
∞	= freestream property

Received Dec. 16, 1992; revision received Jan. 12, 1996; accepted for publication Jan. 26, 1996.

*Mechanical Engineer, Aeromechanics Division, Flight Dynamics Directorate; currently Chief, Aeronautical Sciences, Air Force Office of Scientific Research European Office of Aerospace Research and Development, 223/231 Old Marylebone Road, London NW1 5TH, England, United Kingdom. Senior Member AIAA.

Introduction

LASER Doppler velocimetry (LDV) has proven to be a highly successful nonintrusive, quantitative measurement technique for flow structure analysis as well as computational fluid dynamics (CFD) verification and validation efforts. However, in the analysis of LDV data, it must be recognized that measured velocities are of particles within the flowfield. If the particles do not accurately match the fluid velocities, the measurements are biased and should not be presented as representative of the fluid flow.

LDV measurements containing an unknown quantity of velocity lag bias are still useful for qualitative flowfield analysis, particularly within complex flow structures that may be altered by intrusive probes, such as compression turns[1] or supersonic vortices.[2] However, if the bias is not recognized, published data may be more harmful than beneficial. If the data are utilized by a computationalist who is not familiar with sources of LDV bias, discrepancies between the experimental and computational solutions may be much greater than anticipated, leading to incorrect conclusions about the quality of the measurements or the accuracy of the CFD analysis.

Any quantitative analysis of velocity lag bias requires knowledge of the particle size distribution. For flows using an aerosol as seed material, the average in-tunnel particle size can be measured by a transmissometer[3] or deduced from LDV measured mean velocities downstream of a shock.[4] If the complete distribution is desired, one approach is to use out-of-tunnel instrumentation.[5] However, this assumes that the seed produced is invariant to differences between in-tunnel and out-of-tunnel conditions, such as pressure and temperature. Also, it does not take into account that the LDV system may not detect valid signals from all particles within the flow. In-tunnel particle sizing has been accomplished using phase Doppler anemometry (PDA),[6] a technique that tags each instantaneous velocity measurement with a corresponding particle size but requires hardware and setup beyond conventional LDV and has not yet extended itself into the hypersonic regime.

Solid particles of a known size are also utilized. Some materials, such as polystyrene spheres, are suspended in a carrier solution of alcohol or water. Successful measurements by this technique require knowledge that the carrier has completely evaporated before reaching the optical probe volume and that individual particles do not cluster to form larger seed. Other solid materials, such as SiO_2 or Al_2O_3, can be introduced to the flow using a fluidized-bed-type seeder without a carrier solution, but the particles can be abrasive to model surfaces at high speeds.

The particle sizing technique presented by this study uses conventional LDV measurements in the homogeneous flowfield immediately downstream of an oblique shock. It is similar to commercially available out-of-tunnel systems in that measurements are grouped into bins of defined size ranges rather than calculating a specific size for each particle such as with PDA. However, this method can be applied to any supersonic or hypersonic wind-tunnel flow and can be used to re-examine measurements of previous LDV studies. By determining the particle size distribution, the design of existing seeder systems can be validated, design parameters for future systems can be established, and the amount of velocity bias in existing measurements can be quantified and removed from the LDV data.[7]

Approach

As a specific example of the particle sizing algorithm, LDV measurements through the oblique, leading-edge shock of a hypersonic inlet forebody are examined.

Experimental Data

A schematic of the forebody is shown in Fig. 1. The model is tested at a calibrated freestream Mach number of 5.76 and a freestream Reynolds number of 44.3×10^6 per meter. The compression shock is attached to the leading edge of the model, based on oblique shock theory, and extends downstream at an angle of 14.75 deg. Velocity measurements are obtained at four vertical survey stations that pass through the shock. The primary survey, 1, is located along the model centerline 17.73 cm downstream from the leading edge. Surveys 2, 3, and 4 are located at 20.27 cm. Survey 2 is on the model centerline, and surveys 3 and 4 are ± 1.9 cm spanwise from the centerline to measure the two-dimensionality of the flow. The total width of the model is 40.64 cm.

Velocity measurements are collected using a two-dimensional LDV system in forward scatter mode.[1] Two thousand pairs of instantaneous, coincident velocities are obtained at each measurement location through each survey. The optical diameter of the LDV probe volume is 0.328 mm, and the spacing between measurement is 1.0 mm. The seed material used is 200 centistoke silicon oil, which is atomized and introduced into the stagnation chamber where the temperature is 500 K and the pressure is 4.8 MPa.

Measurement histograms for the first survey location are presented in Figs. 2 and 3. The component of velocity tangential to the shock, Fig. 2, shows that the measured mean velocity is constant across the shock, as predicted by ideal, inviscid theory.[8] The normal component of velocity, on the other hand, is predicted by ideal theory to drop instantaneously across the shock, so that the vector sum of the downstream tangential and normal components is in the direction parallel to the wedge. As seen by the histograms in Fig. 3, however, the measured particles are virtually unaffected by the shock itself. Instead, the particles rely on drag forces downstream of the shock to slow the particle velocities toward the fluid velocity. Since the smaller particles within the polydispersed seed distribution relax more quickly to the fluid velocity, the histograms downstream of the shock are skewed. The particles must travel nearly 20 mm normal to the shock before their mean velocity approximately matches the fluid.

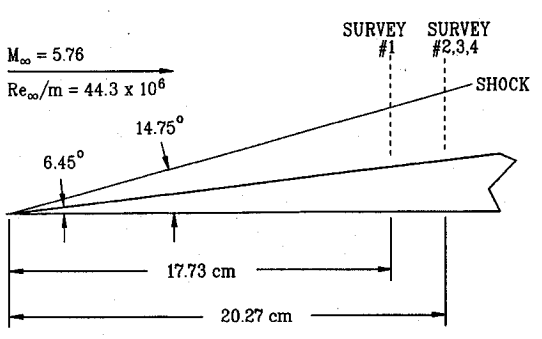

Fig. 1 Two-dimensional schematic of the hypersonic inlet forebody.

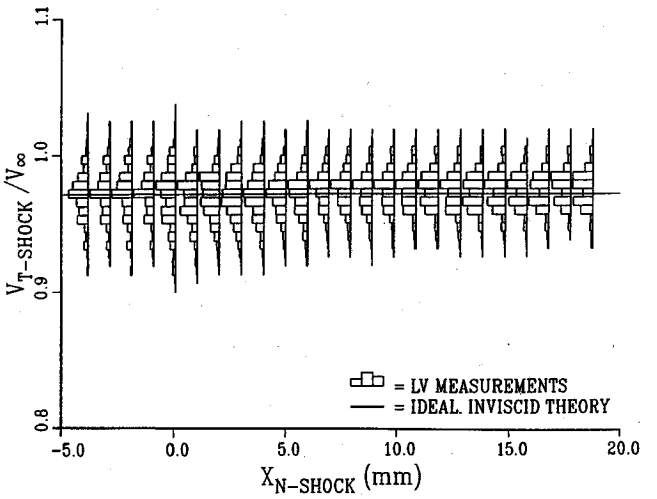

Fig. 2 LDV measured histograms of the velocity component tangential to the shock.

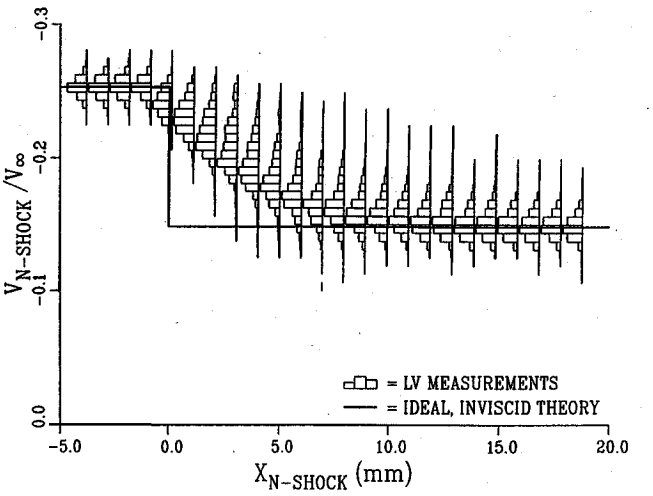

Fig. 3 LDV measured histograms of the velocity component normal to the shock.

Computational Analysis

The velocity lag of particles passing through an oblique shock can be obtained by numerical analysis. Since the flowfield downstream of the shock is ideally uniform and steady state, the equation of motion governing the particle behavior can be written as[4]

$$\frac{dV_{pN-\text{SHOCK}}}{dt} = -\frac{3C_d}{4d}\frac{\rho_f}{\rho_p + \rho_f/2}(V_{pN-\text{SHOCK}} - V_{fN-\text{SHOCK}}) \times |V_{pN-\text{SHOCK}} - V_{fN-\text{SHOCK}}| \quad (1)$$

where the initial velocity of the particle is the normal velocity of the fluid upstream of the shock. To avoid problems with equation stiffness associated with small particle diameters, solutions are obtained by fourth-order Runge–Kutta–Fehlberg (RKF) numerical integration.[9,10] The RKF method combines speed with accuracy by estimating the stiffness of the equation at each time step and then adjusting the step size accordingly. Closure of the equation set is obtained by using the drag law of Crowe[11]:

$$Cd = (C_{d1} - 2)\exp\left[-3.07\gamma^{\frac{1}{2}}(M_R/Re_R)g(Re_R)\right] + \left[h(M_R)\Big/\left(\gamma^{\frac{1}{2}}M_R\right)\right]\exp[-Re_R/(2M_R)] + 2 \quad (2)$$

where

$$C_{d1} = (24/Re_R)\left(1 + 0.158Re_R^{\frac{2}{3}}\right) \quad (3)$$

$$\log_{10} g(Re_R) = 1.25[1 + \tanh(0.77\log_{10} Re_R - 1.92)] \quad (4)$$

and

$$h(M_R) = \left[2.3 + 1.7(T_p/T_f)^{\frac{1}{2}}\right] - 2.3\tanh(1.17\log_{10} M_R) \quad (5)$$

Crowe's drag law is valid over a wide range of relative Reynolds and Mach numbers and includes the effects of inertia, compressibility, rarefaction, and heat transfer.

For the freestream conditions of the inlet forebody, representative numerical calculations for the velocity lag of the silicon oil seed through the leading-edge shock are shown in Fig. 4. The velocity lag downstream of the shock is shown to be strongly dependent on the particle diameter, with the 1.0-μm particles relaxing to within 1% of the fluid velocity at a distance of 8.0 mm normal to the shock, whereas the 10.0-μm particles are barely effected by the shock at the same location.

At any position downstream of the shock, each particle size has an associated mean velocity with an assumed Gaussian probability distribution. Therefore, if the Gaussian functions for each seed size are weighted by their total concentration within the flow, the sum of the functions will match the LDV measured histogram shape at the same location. This concept is demonstrated in Fig. 5. The LDV histogram corresponds to the location 6.9 mm downstream normal from the shock along profile 1. For chosen seed diameters of 1.0, 2.0, and 4.0 μm, concentration weights of 27.4, 63.8, and 8.8%, respectively, allow the three Gaussian functions to be added so that the resulting velocity distribution is the best fit to the experimental data. This approach is similar to decomposing functions into Fourier frequency components. However, unlike Fourier series, the Gaussian functions are a nonorthogonal set; determining the concentrations of each particle size requires the solution of simultaneous equations.[12]

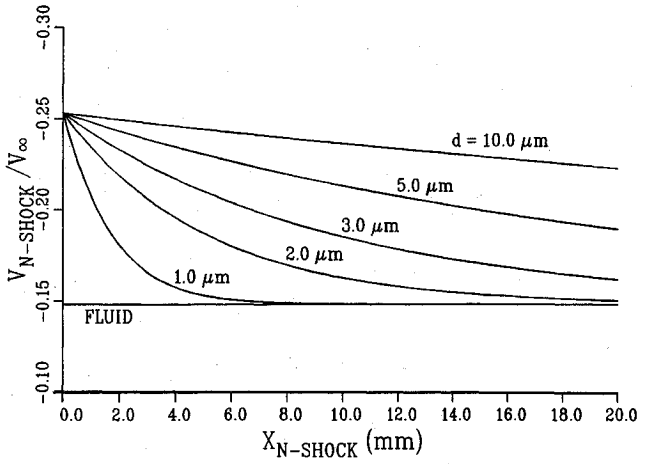

Fig. 4 Calculated velocities for representative particle diameters.

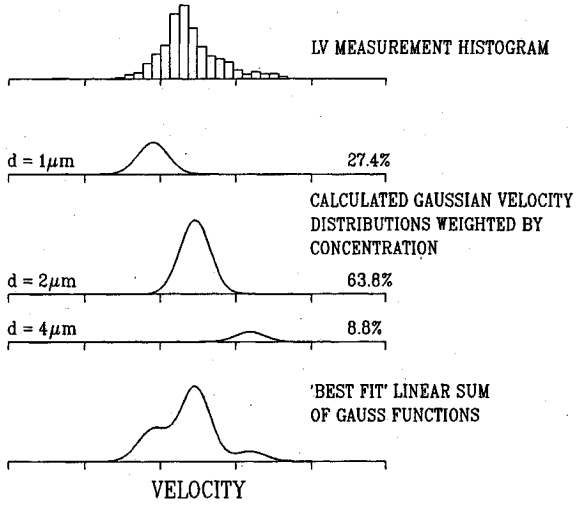

Fig. 5 Least square fit particle sizing by the summation of Gauss functions.

Particle Sizing Algorithm

The concentrations of particle sizes can be obtained by the following algorithm.

1) For an arbitrary number of measurement stations, from $j = 1$ to n_{points}, read in the n_j experimental velocities normal to the shock and create histograms for each data set. Use the same number of equally wide velocity bins for each histogram, from $i = 1$ to n_{bin}, with the median velocity of each bin denoted as V_i and the number of instantaneous measurements within the bin denoted as M_{ij}.

2) Normalize each histogram to have a total integrated area of one:

$$m_{ij} = \frac{M_{ij}}{[n_j \times BW]} \quad (6)$$

3) Choose a representative set of seed diameters d_k, where $k = 1$ to n_{seed}. For each seed diameter, use Eqs. (1–5) to calculate the mean downstream velocity normal to the shock, $\bar{V}_{kj}$, at each of the measurement locations. Using the standard deviation σ of LDV measurements upstream of the shock, the velocity distribution of each seed diameter at each measurement location is described by the normalized Gauss functions:

$$G_{kj}(V) = \frac{1}{(2\pi\sigma^2)^{\frac{1}{2}}}\exp\left[-\frac{(V - \bar{V}_{kj})^2}{2\sigma^2}\right] \quad (7)$$

4) For each seed diameter d_k, let the amount of seed present be denoted as the concentration c_k, where

$$\sum_{k=1}^{n_{\text{seed}}} c_k = 1 \quad (8)$$

If the Gauss functions for each seed diameter could be added so that the experimental histograms are recreated exactly, then for each bin of each histogram

$$\sum_{k=1}^{n_{\text{seed}}} c_k G_{kj}(V_i) = m_{ij} \quad (9)$$

However, if the histograms created by the Gauss functions do not exactly match the experimental histograms, then the difference between the two at each bin is the residual R_{ij}. The total sum of the residuals squared for each bin of each experimental histogram is then

$$R^2 = \sum_{j=1}^{n_{\text{points}}}\sum_{i=1}^{n_{\text{bin}}}\left[m_{ij} - \sum_{k=1}^{n_{\text{seed}}} c_k G_{kj}(V_i)\right]^2 \quad (10)$$

For a least squared error fit of the Gaussian functions to the experimental data, it is desired that the term for R^2 be minimized. With respect to each of the concentrations c_l, R^2 is a parabola, with a minimum value located at

$$\frac{\partial R^2}{\partial c_l} = 0 \quad (11)$$

However, the domain of c_l must be restricted to positive values of seed concentration. As illustrated in Fig. 6, there are two possible equations that specify the minimum R^2 for each c_l. If the apex of the parabola is at a value greater than zero, then the value of c_l that minimizes the residual is identified by Eq. (11). If the apex is at a value of c_l less than zero, then the value of c_l that minimizes the residual is at

$$c_l = 0 \quad (12)$$

By applying the appropriate equation, either Eq. (11) or Eq. (12) for each c_l, a set of n_{seed} simultaneous equations can be solved to yield the concentrations of each seed diameter. In matrix form,

$$\{C\} = [A]^{-1}\{B\} \quad (13)$$

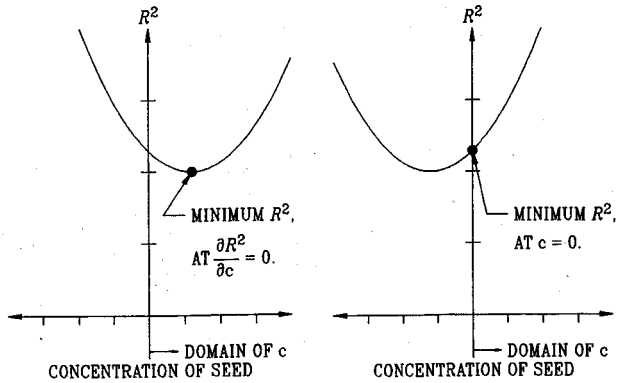

Fig. 6 Minimum squared residual for positive values of seed concentration.

If Eq. (11) is the correct choice for a particular c_l,

$$a_{lk} = \sum_{j=1}^{n_{\text{points}}} \sum_{i=1}^{n_{\text{bin}}} G_{lj}(V_i) G_{kj}(V_i) \tag{14}$$

and

$$b_l = \sum_{j=1}^{n_{\text{points}}} \sum_{i=1}^{n_{\text{bin}}} G_{lj}(V_i) m_{ij} \tag{15}$$

On the other hand, if Eq. (12) is the correct choice for a particular c_l,

$$a_{lk} = \begin{cases} 0, & l \neq k \\ 1, & l = k \end{cases} \tag{16}$$

and

$$b_l = 0 \tag{17}$$

Unfortunately, the correct choice of equations for each c_l depends on the solution. If, for a particular l, the solution yields $c_l > 0$, then Eqs. (14) and (15) were the correct choice. Otherwise, note from Fig. 6 that if $c = 0$ is the minimum within the domain, the slope of the parabola at $c = 0$ is positive. Therefore, if Eqs. (16) and (17) were the correct choice for c_l,

$$\left.\frac{\partial R^2}{\partial c_l}\right|_{c_l = 0} > 0 \tag{18}$$

From Eq. (10), this condition becomes

$$\sum_{j=1}^{n_{\text{points}}} \sum_{i=1}^{n_{\text{bin}}} 2 \left[m_{ij} - \sum_{k=1}^{n_{\text{seed}}} c_k G_{kj}(V_i) \right] \left[-G_{lj}(V_i) \right] \Big|_{c_l = 0} > 0 \tag{19}$$

Based on concentrations solved for when c_l is set equal to zero, Eq. (19) can be rearranged as

$$\sum_{k=1}^{n_{seed}} \left[\sum_{j=1}^{n_{\text{points}}} \sum_{i=1}^{n_{\text{bin}}} G_{lj}(V_i) G_{kj}(V_i) \right] c_k - \left[\sum_{j=1}^{n_{\text{points}}} \sum_{i=1}^{n_{\text{bin}}} G_{lj}(V_i) m_{ij} \right] > 0 \tag{20}$$

For a chosen number of seed diameters, the number of possible equation sets is

$$n_{\text{sets}} = 2^{n_{\text{seed}}} \tag{21}$$

However, only one solution will yield positive values of concentration or satisfy the condition given by Eq. (20) for concentrations equal to zero.

Rather than solving every possible combination of simultaneous equations, the correct solution can be found by relaxation. First, calculate all of the matrix coefficients by using Eqs. (14) and (15), and solve for the various c_l using a method such as Gauss–Jordan elimination.[13] If any of the various c_l are negative, replace the corresponding matrix coefficients by Eqs. (16) and (17) and resolve the concentrations. For each successive solution, a negative value for c_l indicates that row l of the matrix coefficients must be replaced by Eqs. (16) and (17), and any $c_l = 0$ that does not satisfy Eq. (20) indicates that row l of the matrix coefficients must be replaced by Eqs. (14) and (15). This approach will not converge to an incorrect solution but may converge to a limit cycle where the algorithm repeatedly changes the equation sets for the same rows. All solutions for this study, however, did converge to the solution in fewer than 1000 iterations by allowing for a maximum of five changes for each of the first 200 iterations, followed by a single change each time. For a resolution of 40 seed diameters, solving each possible equation set would otherwise require more than 10^{12} solutions.

Results

Single Histogram Analysis

The ability of the particle sizing algorithm to estimate the concentrations of seed diameters from velocity histograms is demonstrated in Figs. 7 and 8. For these examples, a test distribution of particle sizes is numerically tracked through the ideal, inviscid flowfield downstream of the forebody shock. When the particles reach the measurement location at 6.9 mm, the calculated mean velocities and randomly determined velocity fluctuations, based on a Gaussian probability distribution of turbulence, are used to create a set of simulated instantaneous LDV measurements. The simulated measurements are used to create a velocity histogram that is used as input into the particle sizing algorithm. The calculated size distribution from the simulated measurements can then be compared with the input particle diameters. Also, by numerically tracking particles based on the calculated size distribution, a CFD predicted

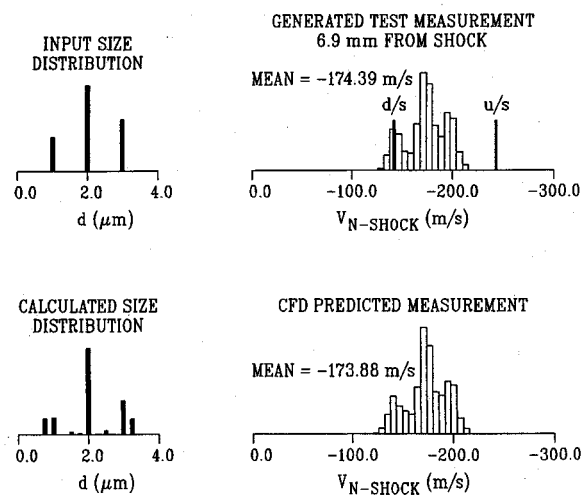

Fig. 7 Test size distribution: three discrete particle diameters.

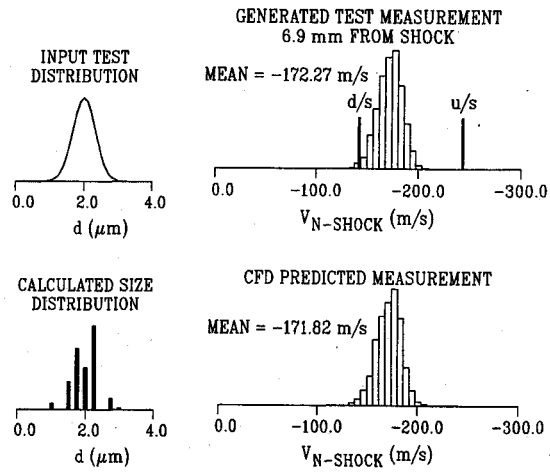

Fig. 8 Test size distribution: Gaussian probability.

velocity histogram is created for comparison to the simulated measurement.

The first example, shown in Fig. 7, is for a test distribution of three discrete particle diameters: 20% at 1.0 μm, 50% at 2.0 μm, and 30% at 3.0 μm. The corresponding simulated measurement histogram shows a trimodel distribution of velocity as the particles relax from the freestream fluid velocity to the velocity behind the shock. The calculated size distribution from the simulated histogram compares very well with the input distribution, with 18.7% at 0.75 or 1.0 μm, 49.6% at 2 μm, and 28.3% at 3.0 or 3.25 μm. The corresponding predicted histogram has a mean value within 0.3% of the simulated measurement and a standard deviation within 0.2%.

Results for a continuous test distribution are shown in Fig. 8. For this case, the size probability function is Gaussian, with a center diameter of 2.0 μm and a standard deviation of 0.333 μm. The calculated size distribution is a good description of the test input, with a mean value of 2.0 μm and a standard deviation of 0.365. The predicted histogram in this case has a mean velocity within 0.3% of the test measurement and a standard deviation within 3.6%.

The particle size distribution based on an actual LDV measurement histogram is shown in Fig. 9. The measurements correspond to the same position and conditions as used for the three test inputs. The size distribution predicted shows 94% of the silicon oil seed to be between 1.75 to 3.0 μm, with the remaining particles as large as 6.5 μm. As with the test distributions, the mean velocity of the measured histogram is very closely predicted by the calculated particle size distribution, within 0.03%, although the standard deviation is underestimated by 14%.

Sensitivity Analysis

Application of the particle sizing algorithm requires the user to define the number of instantaneous LDV measurements to use, the number of measurement histogram bins for sorting the data, the turbulence intensity of the fluid downstream of the shock, and a discrete set of particle diameters. These variables must be chosen with fine enough resolution that the solution will converge. For example, using double the number of measurements should not change the result. To gauge the sensitivity of the predicted mean velocity to these parameters, several additional solutions were calculated for the LDV data used in Fig. 9.

Results of the analysis, shown in Fig. 10, demonstrate that the predicted mean velocities of the LDV measurements through the forebody shock are extremely insensitive to the user-defined parameters. For the measurement histogram, 2000 instantaneous velocities were used to predict the particle sizes and the mean velocity. However, as shown in the figure, the mean velocity prediction varies by a maximum of 1.1% as the number of measurements is decreased to as few as 50.

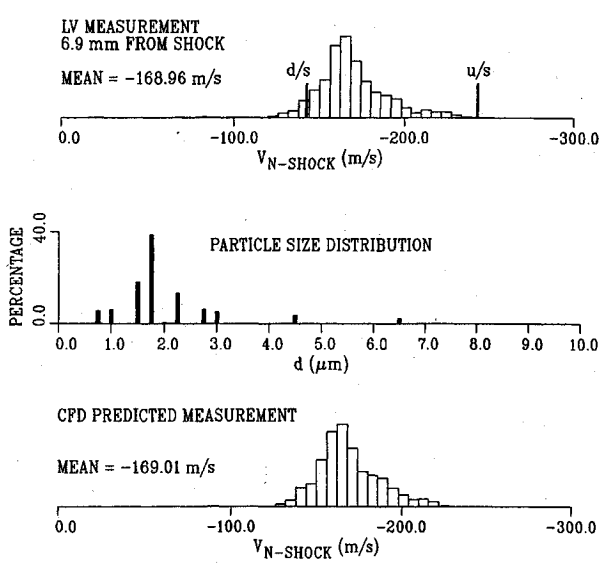

Fig. 9 Particle size distribution based on LDV measurements at a single location downstream of the leading-edge shock.

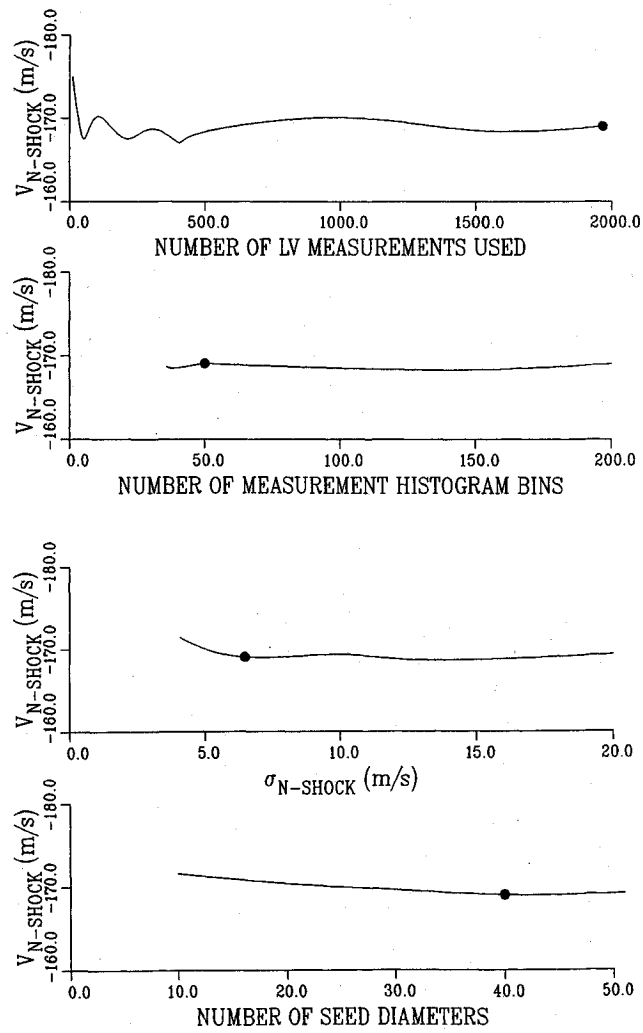

Fig. 10 Sensitivity of the computationally predicted mean velocity: ——, predicted mean and •, baseline value.

The number of measurement histogram bins used to sort the data also has a negligible effect on the predicted mean. For the calculations in Fig. 9, 50 bins were used from zero to 300 m/s. However, the predicted mean varies by less than 0.5% for any number of bins from 36 to 200. It was found that if too few bins are used relative to the total number of particle diameters chosen, the equation set did not converge. In this case, solutions for 35 or less bins required using fewer than the chosen value of 40 seed diameters.

The standard deviation or turbulence intensity of the fluid behind the shock must also be selected. For the data in Fig. 9, a constant value of 6.45 m/s was chosen, based on freestream LDV measurements. Although this ignores turbulence variations as a result of the shock, it is shown that any chosen value from 4.1 to 20 m/s predicts the mean velocity within 1.5%. Values less than 4.1 m/s do not allow the Gaussian functions of the chosen seed diameters to overlap well enough to recreate the LDV measurement. If, for example, the Gaussian functions from two adjacent seed sizes have mean values of 190 and 210 m/s, but both are nearly zero at 200 m/s, the functions cannot be added to represent a nonzero histogram bin at the midway point between them. It is also notable that although the mean value of the resulting particle size distributions varies by less than 6.5% over this range of turbulence intensity, the standard deviation varies as much as 35%. As the turbulence intensity is increased, the resolution of the size distribution decreases towards using as few as three bins for the particle sizes.

The number of seed diameters used to describe the particle size distribution also has little impact on the predicted mean. Although 40 diameters were chosen for the baseline solution, ranging from 0.25 to 10.0 μm, any number from 10 to 50 sizes over the same

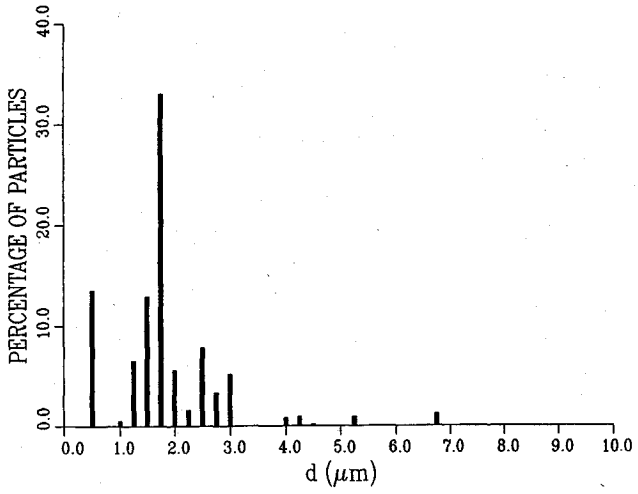

Fig. 11 Particle size distribution based on simultaneous analysis of the 20 LDV histograms downstream of the shock at survey station 1.

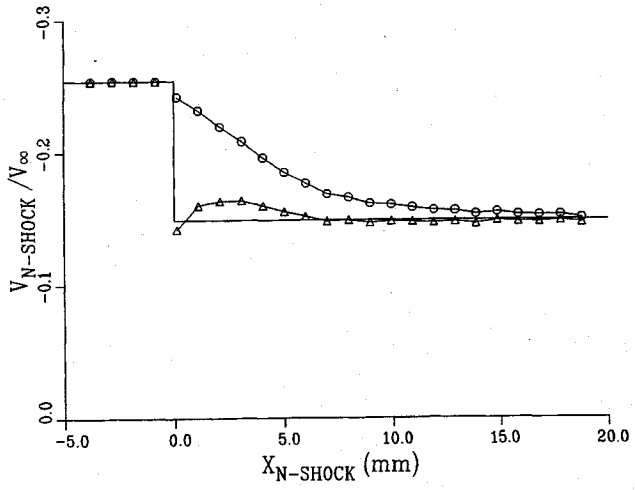

Fig. 12 LDV measured mean velocities at survey station 1, corrected for velocity lag bias: ○, mean velocity of LV measurement; △, corrected LV measurements; and ——, ideal, inviscid theory.

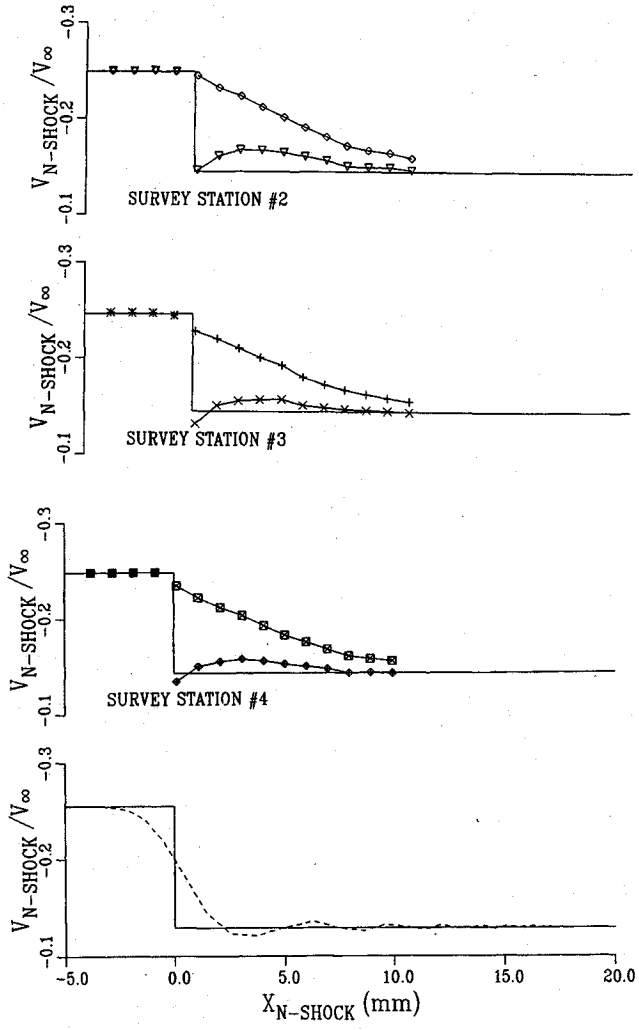

Fig. 13 Measured and corrected mean velocities for survey stations 2, 3, and 4 and a CFD calculated velocity profile: ◇, mean velocity of LDV measurement; ▽, corrected LDV measurements; ——, ideal, invescid theory; +, mean velocity of LDV measurement; ×, corrected LDV measurements; ⊠, mean velocity of LDV measurement; ⊕, corrected LDV measurements; and - - - -, Navier–Stokes CFD calculation.

range yields a mean velocity prediction that varies by only 1.5%. Fewer than 10 diameters cause the same problem as too low of a standard deviation; the Gaussian functions of the adjacent particle sizes do not overlap enough to recreate the histogram shape.

The difference between the predicted mean velocity and the ideal fluid velocity at each measurement location is an estimate of the particle velocity lag bias. By subtracting the estimated bias from each of the measured mean velocities, the corrected velocities can be compared with the ideal, inviscid flow. For the measurements at survey 1, these values are plotted in Fig. 12. Overall, the corrected values agree with the ideal, inviscid theory to within a mean rms difference of 4.2%. Slight deviations, such as the undercorrected measurements nearest the shock, indicate the margin for potential improvement of the experimental data or the computational equation set.

Measured and corrected LDV measurements for surveys 2, 3, and 4 are shown in Fig. 13. In each case, corrections are based on the particle size distribution determined from survey 1. Results show that the corrected measurements are all within 7.5% of the ideal, inviscid velocity prediction. The repeatability of the curves also indicates that there is no significant difference in particle size distribution for the different tunnel runs. The remaining difference between the corrected data and the ideal, inviscid theory is of the same order as can appear in a CFD flowfield prediction. Also shown in Fig. 13 is the velocity predicted by a full Navier–Stokes code that uses artificial viscosity to smear the shock for numerical stability. The oscillation in the curve downstream of the shock yields approximately the same maximum error as the corrected LDV data and dampens out at roughly the same rate.

Conclusions

A numerical algorithm has been presented and demonstrated that can provide an estimate of the particle size distribution of LDV seed by the analysis of velocity histograms downstream of a shock. The method does not require any hardware or data collection beyond conventional LDV measurements and can be applied to existing data sets. It requires that the flow be supersonic but is not otherwise limited by Mach number or Reynolds number. For hypersonic flows, no other method of in-tunnel particle sizing is currently known.

The method was demonstrated using LDV measurements downstream of the leading-edge shock from a hypersonic inlet forebody. A single particle size distribution was found that predicted the velocity bias of all measurements at four separate survey stations. Results were shown to be insensitive to the survey location and to user-specified algorithm parameters.

Knowing the polydispersed size distribution from the forebody shock measurements allows the velocity bias of other measurements throughout the inlet to be quantified by numerically tracking the particles through a companion CFD flowfield prediction. Quantifying the measurement bias greatly enhances the value of LDV as a CFD code validation tool, since the magnitude of this bias can result in substantial differences between raw LDV measurements and the actual aerodynamic flowfield.

Acknowledgments

The author thanks Dean Miller, George Seibert, Linda Smith, and Charles Tyler, each of whom contributed towards the collection and processing of the LDV data.

References

[1]Maurice, M. S., and Seibert, G. L., "LV Measured Turbulent Structure of Mach 6 Flow over a Roughened Flat Plate with a Compression Ramp," AIAA Paper 89-2164, July 1989.

[2]Smith, L. G., Maurice, M. S., Seibert, G. L., and Tyler, C., "Laser Velocimetry Measurements of Supersonic Vortex Flows on a Simple Razor-Edged Delta Wing," AIAA Paper 91-1684, June 1991.

[3]Alvi, F. S., and Settles, G. S., "Physical Model of the Swept Shock/Boundary Layer Interaction Flowfield," AIAA Paper 91-1768, June 1991.

[4]Maurice, M. S., "Method to Quantify and Correct Particle Velocity Bias in Laser Velocimetry Measurements," AIAA Paper 92-0764, Jan. 1992.

[5]Parobek, D. M., Boyer, D. L., and Clinehens, G. A., "Recent Developments in Liquid Flow Seeding Techniques for Use with LV Measurements," AIAA Paper 86-0769, March 1986.

[6]Rudoff, R. C., and Bachalo, W. D., "Seed Particle Response and Size Characterization in High Speed Flows," *Laser Anemometry—Advances and Applications*, American Society of Mechanical Engineers, New York, 1991 pp. 443–448

[7]Maurice, M. S., "Quantitative Laser Velocimetery Measurements in the Hypersonic Regime by the Integration of Experimental and Computational Analysis," AIAA Paper 93-0089, Jan. 1993.

[8]Zucker, R. D., *Fundamentals of Gas Dynamics*, Matrix, Beaverton, OR, 1977, pp. 176–181.

[9]Mathews, J. H., *Numerical Methods for Computer Science, Engineering, and Mathematics*, Prentice–Hall, Englewood Cliffs, NJ, 1987, pp. 429, 430.

[10]Bordon, L. R., and Faires, J. D., *Numerical Analysis*, Prindle, Weber and Schmidt, Boston, MA, 1989, pp. 252–255.

[11]Crowe, C. T., "Drag Coefficient of Particles in a Rocket Nozzle," *AIAA Journal*, Vol. 5, No. 5, 1967, pp. 1021, 1022.

[12]Powers, D. L., *Boundary Value Problems*, 2nd ed., Academic, New York, 1979, pp. 30–33, 47, 48.

[13]Hildebrand, F. B., *Methods of Applied Mathematics*, Prentice–Hall, Englewood Cliffs, NJ, 1965, pp. 1–4.